Hindawi
International Journal of Optics
Volume 2019, Article ID 2936172, 10 pages
https://doi.org/10.1155/2019/2936172

Research Article

Holographic Interferometer for the Study of Phase Media, Which Has Four Output Channels of Different Sensitivity

Yusupzhan Kh. Ismanov and Nasipbek K. Dzhamankyzov

Institute of Physical & Technical Problems and Materials Science of National Academy of Sciences of Kyrgyz Republic, Bishkek 720071, Kyrgyzstan

Correspondence should be addressed to Yusupzhan Kh. Ismanov; i_yusupjan@mail.ru

Received 20 September 2018; Revised 17 November 2018; Accepted 25 November 2018; Published 1 January 2019

Academic Editor: Wonho Jhe

Computer simulation of the interferometer combining properties of low-sensitive Talbot interferometer and high-sensitive holographic interferometer is considered. The interferometer has four output channels having different sensitivity. Channel sensibility can be varied by means of spatial filtration. The base of the interferometer is the holographic Talbot effect. The efficiency of this interferometer was verified by computer simulation method. Some results of the computer simulation are presented in the article. These results were compared with results obtained in optical experiments under the same conditions. A wide range of sensitivity of the interferometer makes it possible to use the interferometer to study complex phase objects, primarily dynamic media.

1. Introduction

The study and control of the characteristics of high-temperature plasma and aerodynamic experiments, the study of distributions of densities and temperatures in reservoirs, etc. are areas in which it is impossible to do without the use of interferometry methods. However, it is during the study of these media that one, but rather significant, shortcoming of the known interferometry methods is manifested; they all can work only at one, given sensitivity value. But to study the above-mentioned complex phase media of a dynamic nature, interferometers of different sensitivity are required. Only in this case it is possible to obtain comprehensive interferometric information about these media. And for media of a dynamic nature, these interferometers must be used simultaneously to receive information at any time for different sensitivity values. However, the difficulties associated with the temporal consistency of the operation of the interferometer complex greatly complicate the interferometric control systems and the measurements intended for these media. From this point of view, it becomes very urgent to develop an interferometer that allows real-time information retrieval both at low-sensitivity levels and in the highly sensitive mode of a holographic interferometer.

In this paper we consider a model of a four-channel holographic interferometer whose two output channels form a low-frequency moiré pattern due to the Talbot effect [1–10]; that is, they work as a Talbot interferometer [11–19]. These are channels of low sensitivity. The other two output channels are highly sensitive holographic channels. The basis of the interferometer is the holographic Talbot effect [20–22].

To date, many methods have been proposed for studying the characteristics of phase media, such as, for example, the distribution of temperature fields [23–25]. However, the measurement methods proposed in these works are based on the methods of holographic interferometry with a single output channel, which limits their ability to measure in complex phase media, with a continuously changing pattern of temperature distribution. In work [26], in which, to obtain information on the temperature distribution of the flame of a candle, a shear holographic lens is used, four almost identical interferograms are obtained at the output, which is associated with the features of the optical scheme. For information on the distribution of the temperature field of a candle flame, the authors use one of them. That is, in fact, it is a single-channel interferometer. The interferometer offered by us, as we have already mentioned, has four output

channels of different sensitivity; i.e., the information of any of the channels complements the information obtained in other channels and is not their repetition.

2. Theoretical Base of the Wide-Range Holographic Interferometer

A multichannel wide-range holographic interferometer is an interferometer that combines the best characteristics of the Talbot interferometer and the holographic interferometer. The basis of the interferometer is the holographic effect of Talbot [22]. It has been shown experimentally that the restoration of the bleached hologram of a one-dimensional grating by a coherent reference wave forms imaginary and real images of the grating and its self-reproductions in the ± 1-th diffraction orders. It was found that this sequence of self-reproductions is also reconstructed in the 0-th diffraction order (Figure 1). In all the diffraction orders, the sequences of imaginary images of the grating self-reproductions are continued by a sequence of real images of the self-reproductions of this grating. This fact makes it possible to observe these sequences without using special optics. The holographic effect of Talbot can be used in the construction of a holographic interferometer [27–29]. The prototype of the four-channel wide-range holographic interferometer is the Talbot interferometer [11], which consists of two linear gratings separated by a distance multiple of the Talbot constant $z_T = 2d^2/\lambda$ (Figure 2).

The phase object under consideration is placed between these gratings. Interference pattern which is produced on the screen gives us information about the phase object. In contrast to the Talbot interferometer in a holographic interferometer, a photographic plate is placed in place of the second grating (Figure 3). When the photographic plate is simultaneously illuminated by a plane reference wave incident at an angle θ to the plane of the plate, we obtain a hologram of a complex object-a linear grating plus a phase object. Moreover, when recording a hologram, the distance between the grating and the plane of the photographic plate is arbitrary. The distances between the phase object and the grating and object and plane of the photographic plate are also arbitrary. Consider the process of recording the hologram in more detail. For a one-dimensional grating placed in the coordinate plane (x_0, y_0), the transmittance is

$$t(x_0) = \sum_{m=-\infty}^{\infty} c_m \exp\left(\frac{i2\pi x_0 m}{d}\right). \quad (1)$$

Here, d is the grating period.

We illuminate the grating by a plane wave propagating along the Z axis and having unit amplitude $u(x_0, y_0, z_0^-) = \exp(ikz_0)$. Here $k = 2\pi/\lambda$. Consider $z_0 = 0$; i.e., the plane passes through the origin of the Z axis; we obtain for the wave incident on the grating,

$$u(x_0, y_0 z_0^-) = 1. \quad (2)$$

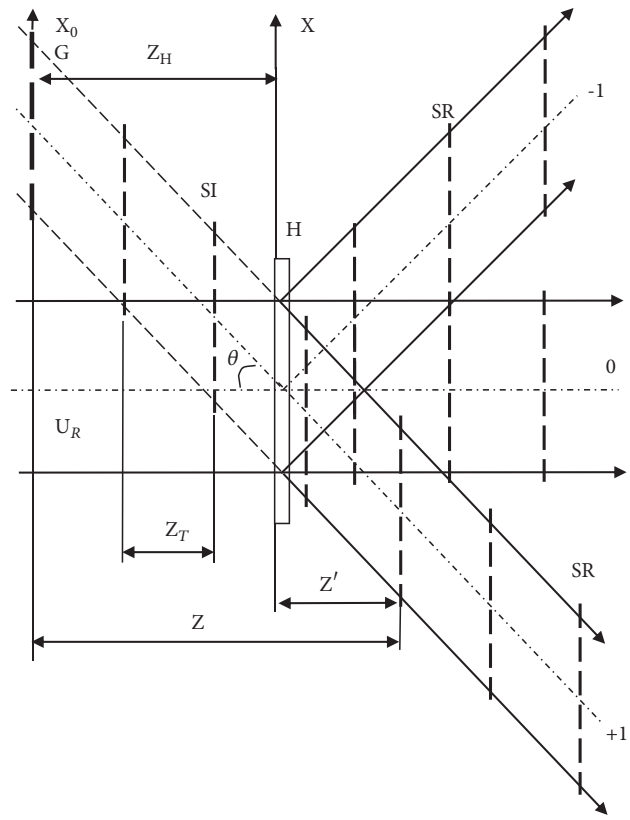

Figure 1: Reconstruction scheme for the hologram of the one-dimensional grating. G is the imaginary image of the grating, SI are positions of imaginary images of self-reproductions, SR are positions of real images of self-reproductions, H is a hologram, and U_R is the reference wave.

In this case, the field immediately after the grating has the form

$$u(x_0, y_0, z_0^+) = u(x_0, y_0, z_0^-)\, t(x_0) = \sum_{m=-\infty}^{\infty} c_m \exp\left(\frac{i2\pi x_0 m}{d}\right). \quad (3)$$

The field at some distance z_1 from the grating is

$$u(x_1, y_1, z_1^-) = 0.5 \exp(ikz_1) \cdot \sum_{m=-\infty}^{\infty} c_m \exp\left[i2\pi\left(\frac{x_1 m}{d} - \frac{m^2 \lambda z_1}{2d^2}\right)\right]. \quad (4)$$

The phase object $u_0(x_1, y_1)$ is located in the plane (x_1, y_1). For simplicity, consider a two-dimensional object. In this case, the field immediately after the object is equal to

$$u(x_1, y_1, z_1^+) = u(x_1, y_1, z_1^-)\, u_0(x_1, y_1) \quad (5)$$

We use the Gabor method for splitting the grating transmission function into a constant component (with zero spatial frequency) $a_0 = c_0$ and a diffracted component with a nonzero spatial frequency $a_m(x_0, z_0) =$

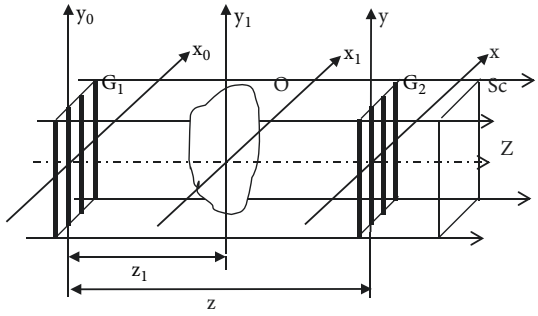

Figure 2: The scheme of the ordinary Talbot interferometer. Here G_1 and G_2 are linear one-dimensional gratings, Ob is the phase object, Sc is a screen, z is the distance between gratings G_1 and G_2, and z_1 is the distance between grating G_2 and screen Sc. z and z_1 are multiples of $z_T = 2d^2/\lambda$. (Here d is the grating period, λ is the wavelength of the incident light.)

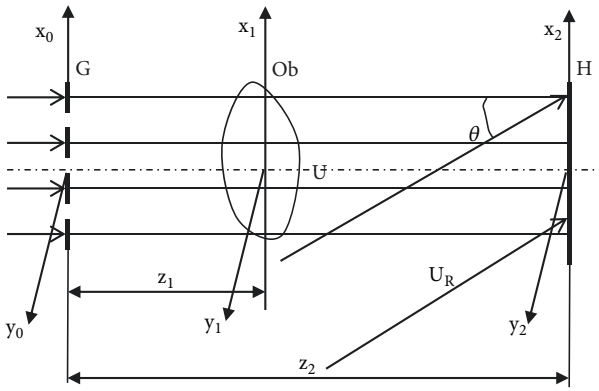

Figure 3: The scheme of recording of a phase object hologram in the four-channel wide-range holographic interferometer. U_R is a reference wave, U is an object wave, G is a grating, Ob is a phase object, H is a hologram, and θ is an incident angle of the reference wave.

$\sum_{m=-\infty,m\neq 0}^{\infty} c_m \exp[i2\pi(x_0 m/d)$. At a distance z_1 from the grating plane $a_m(x_1, z_1) = \sum_{m=-\infty,m\neq 0}^{\infty} c_m \exp[i2\pi(x_1 m/d - m^2\lambda z_1/2d^2)]$. In this case, the field at a distance z_1 from the grating is

$$u\left(x_1, y_1, z_1^-\right) = 0.5c_0 \exp\left(ikz_1\right) + 0.5\exp\left(ikz_1\right) \cdot \sum_{m=-\infty,m\neq 0}^{\infty} c_m \exp\left[i2\pi\left(\frac{x_1 m}{d} - \frac{m^2\lambda z_1}{(2d^2)}\right)\right]. \quad (6)$$

By analogy, we represent the transmission function of the phase object $t(x, y)$, at a distance z_1 from the grating as $t(x_1, y_1) = t_0 + \Delta t(x_1, y_1)$, where t_0 and $\Delta t(x_1, y_1)$, respectively, are the undiffracted and diffracted components of light field immediately behind the object. Now the field directly behind the phase object can be represented in the form

$$\begin{aligned} u\left(x_1, y_1, z_1^+\right) &= 0.5\exp\left(ikz_1\right)c_0 t_0 \\ &+ t_0 \sum_{m=-\infty,m\neq 0}^{\infty} c_m \exp\left[i2\pi\left(\frac{x_1 m}{d} - \frac{m^2\lambda z_1}{2d^2}\right)\right] \times \\ &\times 0.5\exp\left(ikz_1\right) + 0.5\exp\left(ikz_1\right)c_0\Delta t\left(x_1, y_1\right) \\ &+ \Delta t\left(x_1, y_1\right) \sum_{m=-\infty,m\neq 0}^{\infty} c_m \times \\ &\times \exp\left[i2\pi\left(\frac{x_1 m}{d} - \frac{m^2\lambda z_1}{2d^2}\right)\right] 0.5\exp\left(ikz_1\right) \end{aligned} \quad (7)$$

The field at some distance $\Delta z = z_2 - z_1$ from the object is equal in the paraxial approximation to the Fresnel transformation from $u(x_1, y_1, z_1^+)$. For the first term in (7), the Fresnel transform has the form

$$\begin{aligned} Q_1 &= 0.5\frac{\exp\left(ikz_2\right)}{i\lambda\left(z_2 - z_1\right)}c_0 t_0 \exp\left[\frac{ik\left(x_2^2 + y_2^2\right)}{2\left(z_2 - z_1\right)}\right] \\ &\cdot \int_{\infty} \exp\left[\frac{ikx_1^2}{2\left(z_2 - z_1\right)}\right] \times \\ &\times \exp\left[\frac{ik}{2\left(z_2 - z_1\right)}2x_2 x_1\right] dx_1 \int_{\infty} \exp\left[\frac{iky_1^2}{2\left(z_2 - z_1\right)}\right] \\ &\cdot \exp\left[\frac{ik}{2\left(z_2 - z_1\right)}2y_2 y_1\right] dy_1. \end{aligned} \quad (8)$$

$$\begin{aligned} A &= \int_{\infty} \exp\left[\frac{ikx_1^2}{2\left(z_2 - z_1\right)}\right] \\ &\cdot \exp\left[\frac{ik}{2\left(z_2 - z_1\right)}2x_2 x_1\right] dx_1 = \sqrt{\lambda\left(z_2 - z_1\right)} \\ &\cdot \exp\left(\frac{i\pi}{4}\right)\exp\left[-i\frac{\pi}{\lambda\left(z_2 - z_1\right)}x_2^2\right]. \end{aligned} \quad (9)$$

Integral A is a one-dimensional Fourier transform. When integrating, we used the properties of the Fourier transform.

$$\begin{aligned} B &= \int_{\infty} \exp\left[\frac{iky_1^2}{2\left(z_2 - z_1\right)}\right]\exp\left[\frac{ik}{2\left(z_2 - z_1\right)}2y_1 y_2\right] dy_1 \\ &= \sqrt{\lambda\left(z_2 - z_1\right)}\exp\left(\frac{i\pi}{4}\right)\exp\left[-i\frac{\pi}{\lambda\left(z_2 - z_1\right)}y_2^2\right]. \end{aligned} \quad (10)$$

Integral B is analogous to integral A. Product $A \cdot B$ equals

$$A \cdot B = i\lambda\left(z_2 - z_1\right)\exp\left[-i\frac{k\left(x_2^2 + y_2^2\right)}{2\left(z_2 - z_1\right)}\right] \quad (11)$$

Q_1, according to (8), is equal to

$$Q_1 = 0.5\frac{\exp(ikz_2)}{i\lambda(z_2 - z_1)}c_0 t_0 \exp\left[\frac{ik\left(x_2^2 + y_2^2\right)}{2(z_2 - z_1)}\right] A \cdot B = 0.5\exp(ikz_2)\, c_0 t_0. \tag{12}$$

Expression (12) shows that the nondiffracted component with zero frequency is present in the wave incident on the photographic plate, and this is a plane wave whose direction coincides with the direction of the original plane wave illuminating the grating.

Consider the second term in (7):

$$Q_2 = \frac{\exp[ik(z_2 - z_1)}{i\lambda(z_2 - z_1)}\iint_{\infty} 0.5\exp(ikz_1)\, t_0 \cdot \sum_{m=-\infty, m\neq 0}^{\infty} c_m \times \times \exp\left[i2\pi\left(\frac{x_1 m}{d} - \frac{m^2\lambda z_1}{2d^2}\right)\right. \cdot \exp\left\{\frac{ik}{2(z_2 - z_1)}\left[(x_2 - x_1)^2 + (y_2 - y_1)^2\right]\right\} dx_1 dy_1. \tag{13}$$

We take out the multipliers that are independent of the variable of integration:

$$Q_2 = 0.5\frac{\exp(ikz_2)}{i\lambda(z_2 - z_1)}t_0 \sum_{m=-\infty, m\neq 0}^{\infty} c_m \exp\left(-i2\pi\frac{m^2\lambda z_1}{2d^2}\right) \cdot \iint_{\infty} \exp\left(i\frac{2\pi x_1 m}{d}\right)\times \times \exp\left\{\frac{ik}{2(z_2 - z_1)}\left[(x_2 - x_1)^2 + (y_2 - y_1)^2\right]\right\} dx_1 dy_1. \tag{14}$$

After a series of transformations, expression (14) takes the following form:

$$Q_2 = 0.5\exp(ikz_2)\, t_0 \sum_{m=-\infty, m\neq 0}^{\infty} c_m \exp\left(-i2\pi\frac{m^2\lambda z_1}{2d^2}\right)\times \times \exp\left\{i2\pi\left[\frac{x_2 m}{d} - \frac{m^2\lambda(z_2 - z_1)}{2d^2}\right]\right\} = 0.5 \cdot \exp(ikz_2)\, t_0 \sum_{m=-\infty, m\neq 0}^{\infty} c_m \cdot \exp\left[i2\pi\left(\frac{x_2 m}{d} - \frac{m^2\lambda z_2}{2d^2}\right)\right]. \tag{15}$$

As can be seen from (15), this component carries information about the grating, since its amplitude and phase change periodically in the (x, y) plane in accordance with the change of these characteristics in the field immediately after the initial grating. At distances of multiples of $2d^2/\lambda$, this field forms accurate images of the grating - self-reproductions.

The third term in (7) has the form

$$Q_3 = c_0\frac{\exp(ikz_2)}{2i\lambda(z_2 - z_1)}\iint_{\infty} \Delta t(x_1, y_1) \cdot \exp\left\{\frac{ik}{2(z_2 - z_1)}\left[(x_2 - x_1)^2 + (y_2 - y_1)^2\right]\right\} dx_1 dy_1 \tag{16}$$

The term Q_3, as seen from (16), carries the basic information about the phase object, since it is the component $\Delta t(x_1, y_1)$ of the transmission coefficient that is an indicator of the phase distortions introduced by the object.

The fourth term can be represented in the following form:

$$Q_4 = \frac{\exp(ikz_2)}{2i\lambda(z_2 - z_1)}\iint_{\infty} \Delta t(x_1, y_1) \sum_{m=-\infty, m\neq 0}^{\infty} c_m \cdot \exp\left[i2\pi\left(\frac{x_1 m}{d} - \frac{m^2\lambda z_1}{2d^2}\right)\right]\times \times \exp\left\{\frac{ik}{2(z_2 - z_1)}\left[(x_2 - x_1)^2 + (y_2 - y_1)^2\right]\right\} dx_1 dy_1 \tag{17}$$

The last term in (7) is the image of the grating distorted by the phase medium located between the grating and the photographic plate. In this case, it is these distortions, fixed by the photographic plate, that will carry additional information about the optical inhomogeneities of the phase medium. From what has been said above, we can conclude that the object wave incident on a photographic plate is a superposition of four waves:

$$Q = Q_1 + Q_2 + Q_3 + Q_4 \tag{18}$$

To separate in space the real and imaginary images of the object that arise when the hologram is reconstructed, the photographic plate when recording the hologram is also illuminated by a plane reference wave of the form

$$u_R = A\exp(-i\psi), \tag{19}$$

where $\psi = (x_2\sin\theta + y_2\cos\theta\cos\varphi + z_2\cos\theta\sin\varphi)2\pi/\lambda$ phase of a plane reference wave whose propagation direction makes an angle θ with a plane (y_2, z_2) and an angle φ with a plane (x_2, y_2). If we confine ourselves to the one-dimensional case, then the angle $\varphi = \pi/2$ and the phase of the plane wave is $\psi = (x_2\sin\theta + z_2\cos\theta)$.

The intensity distribution in the plane of the hologram is determined by the following relation:

$$I = Q_1Q_1^* + Q_1Q_2^* + Q_1Q_3^* + Q_1Q_4^* + Q_1Ae^{i\psi} + Q_2Q_1^* + Q_2Q_2^* + Q_2Q_3^* + Q_2Q_4^* + Q_2Ae^{i\psi} + + Q_3Q_1^* + Q_3Q_2^* + Q_3Q_3^* + Q_3Q_4^* + Q_3Ae^{i\psi} + Q_4Q_1^* + Q_4Q_2^* + Q_4Q_3^* + Q_4Q_4^* +$$

$$+ Q_4 A e^{i\psi} + Q_1^* A e^{-i\psi} + Q_2^* A e^{-i\psi} + + Q_3^* A e^{-i\psi} + Q_4^* A e^{-i\psi} + A^2 \tag{20}$$

Let us consider the case of a purely phase object. The transmittance of such a medium can be represented as $t(x, y) = \exp[i\varphi(x, y)]$, where $\varphi(x, y)$ is the function describing the phase change in the plane of the object. For the medium, it is characteristic that the contribution of the nondiffracted component is very insignificant; that is, we can assume that $Q_2 = Q_1 = 0$ and $t(x, y) \approx \Delta t(x, y)$. It follows that when the linear registration and processing conditions of the hologram are satisfied, its transmittance, within a constant multiplier, is proportional to the intensity distribution in the hologram plane, which for the purely phase object has the form

$$I = Q_3 Q_3^* + Q_3 Q_4^* + Q_3 A e^{i\psi} + Q_4 Q_3^* + Q_4 Q_4^* + Q_4 A e^{i\psi} + Q_3^* A e^{-i\psi} + Q_4^* A e^{-i\psi} + A^2. \tag{21}$$

Consider the process of reconstructing such a hologram. When the hologram is reconstructed, it is illuminated simultaneously by the initial reference wave and by the wave which was distorted by changes in the phase object. This object wave can be represented in the following form: $Q' = Q_3' + Q_4'$. For a modified object, the transmission function can be represented in the form

$$t'(x, y) = \exp\{i[\phi(x, y) + \Delta\phi(x, y)]\}. \tag{22}$$

Q_3' and Q_4' have the same form as Q_3 and Q_4 in relations (16) and (17), but instead of $\Delta t(x, y) = t(x, y)$ we substitute $\Delta t'(x, y) = t'(x, y)$.

In the reconstructing object wave, the original grating can be rotated by a small angle α in the (x, y) plane, which increases the sensitivity of the channels.

As a result of the reconstruction of the hologram immediately after the hologram, a field of the following type is formed:

$$\begin{aligned} u = I\left(Q_3' + Q_4' + Ae^{-i\psi}\right) &= \left(Q_3^* A^2 + Q_4^* A^2\right) e^{-i2\psi} \\ &+ \left(Q_3^* Q_3' A + Q_4^* Q_3' A + \right. \\ &+ Q_3^* Q_4' A + Q_4^* Q_4' A + Q_3 Q_3^* A + Q_3 Q_4^* A + Q_4 Q_3^* A \\ &\left. + Q_4 Q_4^* A + A^3\right) e^{-i\psi} + \\ &+ \left(Q_3 Q_3^* Q_3' + Q_3 Q_4^* Q_3' + Q_4 Q_3^* Q_3' + Q_4 Q_4^* Q_3' \right. \\ &+ A^2 Q_3' + Q_3 Q_3^* Q_4' + Q_3 Q_4^* Q_4' + \\ &\left. + Q_4 Q_3^* Q_4' + Q_4 Q_4^* Q_4' + A^2 Q_4' + Q_3 A^2 + Q_4 A^2\right) e^{i0} \\ &+ \left(Q_3 Q_3' A + Q_4 Q_3' A + Q_3 Q_4' A + Q_4 Q_4' A\right) e^{i\psi} \end{aligned} \tag{23}$$

As can be seen from (23), the hologram produces four waves whose propagation directions are determined by the phases $-2\psi, -\psi, 0$ and ψ.

If you place the screens in the plane (x_2, y_2) in the path of these rays, then on these screens you will see interference patterns. The centers of these patterns are shifted relative to the z-axis by $-2x_2 \sin\theta$, $-x_2 \sin\theta$, and 0, respectively, where θ is the angle of incidence of the reference wave.

If we designate these rays in the above sequence as numbers I, II, III, and IV, respectively, they can be considered as output channels I, II, III, and IV of a holographic interferometer (Figure 4). Let us consider in more detail the field distributions in directions I, II, III, and IV.

(1) Direction I is determined by the component

$$u_I = \left(Q_3^* + Q_4^*\right) A^2 = \left(Q_3 + Q_4\right)^* A^2 e^{-i2\psi}. \tag{24}$$

As can be seen from (24), in this direction, the conjugate real image of the original, complex object is reconstructed: a linear grating plus an unchanged phase object. On the screen placed in the path of the ray I an image of the original grating appears, distorted by the initial phase object. From the distortions of the grating image on the screen, one can estimate the kind of distribution of optical inhomogeneity in the phase object. This channel of the interferometer can be used for a rather rough estimate of the initial phase object and, in fact, it is the channel in which the Ronchi method is used.

(2) In direction II, the field is determined, according to (23), by the relation

$$\begin{aligned} u_{II} &= Q_3{}^* Q_3' A + Q_4^* Q_3 A + Q_3^* Q_4' A + Q_4^* Q_4 A \\ &+ Q_3 Q_3^* A + \\ &+ Q_3 Q_4^* A + Q_4 Q_3^* A + Q_4 Q_4^* A + A^3 = \\ &= \left[\left(Q_3 + Q_4\right)^* \left(Q_3 + Q_4 + Q_3' + Q_4'\right) + A^2\right] A \end{aligned} \tag{25}$$

The factor $Q_3 + Q_4 + Q_3' + Q_4'$ is a superposition of two (original and modified) images of an object in a real area of space. This multiplier generates an interferogram that carries information about the change of the phase object. However, the picture is complicated by the fact that the result of the superposition of the two images is correlated by the factor $(Q_3 + Q_4^*)$, which is a conjugate image of the original object (phase object plus a linear grating). In this channel we obtain a holographic interferogram modulated by a linear grating, i.e., picture of moiré. The effect of the background term A^3 is eliminated when the hologram is bleached.

In addition to the image of a linear grating, the whole sequence of its self-reproductions (the Talbot effect) is also restored in this direction. Therefore, by placing a screen in any of the planes of self-reproduction, you can fix a clear interference pattern.

From what has been said, it can be seen that this direction represents a highly sensitive holographic channel, since here the addition of initial and modified objects occurs. This is a highly sensitive component of this channel, allowing registering very weak changes in the distribution of inhomogeneity in the phase object. To select this component of the channel you

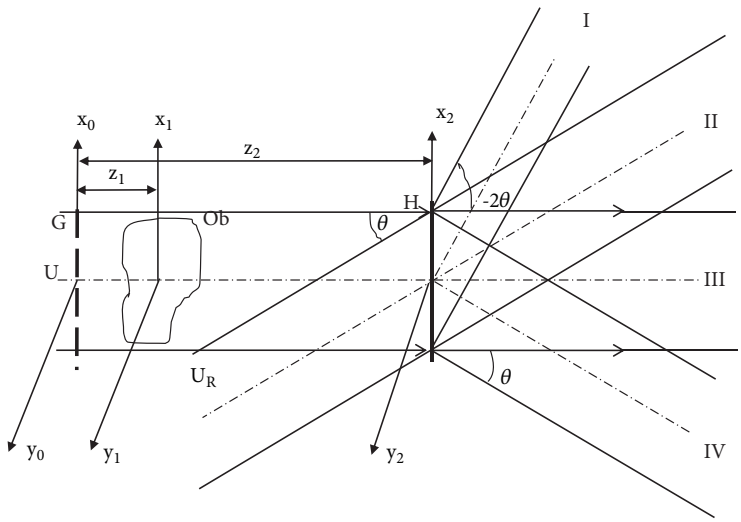

FIGURE 4: The scheme of the hologram reconstruction. U is an object wave, U_R is a plane reference wave, G is a one-dimensional grating, and Ob is an object. There are four waves behind the hologram. They are numbered as I, II, III, and IV.

can use high-frequency filtering methods. The moiré pattern, which arises from the presence of a linear grating between planes of a phase object and the hologram, is a low-sensitivity channel component. This component of the channel makes it possible to obtain information about the regions with a sharp change in the refractive index of the phase medium. This channel component can be extracted by low-frequency filtering methods, for example, by defocusing the image of the interferogram at the channel output.

(3) The third channel of the interferometer is determined by a term representing the zero order of diffraction in expression (23):

$$\begin{aligned} u_{III} &= Q_3 Q_3^* Q_3' + Q_3 Q_4^* Q_3' + Q_4 Q_3^* Q_3' + Q_4 Q_4^* Q_3' \\ &\quad + A^2 Q_3' + Q_3 Q_3^* Q_4' + \\ &+ Q_3 Q_4^* Q_4' + Q_4 Q_3' Q_4' + Q_4 Q_4^* Q_4' + A^2 Q_4' + Q_3 A^2 \\ &\quad + Q_4 A^2 = \\ &= \left(Q_3' + Q_4'\right)(Q_3 + Q_4)(Q_3 + Q_4)^* \\ &\quad + A^2 \left(Q_3 + Q_4 + Q_3' + Q_4'\right) \end{aligned} \tag{26}$$

The second term in (26) is the sum of the images of the original and modified objects. This term represents the holographic interference pattern.

The term $(Q_3' + Q_4')(Q_3 + Q_4)(Q_3 + Q_4)^*$, which is a correlation of the modified phase object of the amplitude component of the original object, is responsible for the occurrence of a low-frequency moiré against the background of a high-frequency holographic interference pattern. High-frequency and low-frequency components in a given channel can be detected using high-frequency and low-frequency filtering techniques. It can also be seen from (26) that the problem of information reading in a given channel is solved by an accurate determination of the planes of self-reproduction of the grating and by the placement in them of either a screen or a photographic plate. It is in these planes that the most clear interference pattern appears.

(4) The fourth channel is determined by the term

$$\begin{aligned} u_{IV} &= \left(Q_3 Q_3' + Q_3 Q_3' + Q_3 Q_4' + Q_4 Q_4'\right) A \\ &= (Q_3 + Q_4)\left(Q_3' + Q_4'\right) A \end{aligned} \tag{27}$$

This channel is a conventional Talbot interferometer. This is especially evident if the hologram of the original object and the grating is reconstructed by a reference wave and an object wave in which only the original grating is left and the phase object is removed. The grating in the reconstructing wave can be rotated about an axis that runs perpendicular to the plane of the lattice, which makes it possible to change the sensitivity of the channel. In this channel, the distribution of phase object inhomogeneity is estimated only by means of low-frequency moiré, so this channel has low sensitivity.

3. Results of the Computer Simulation of the Wide-Range Holographic Interferometer

On the basis of the considered mathematical model, a computer model of a four-channel holographic interferometer was realized. Some results of the computer simulation of the four-channel holographic interferometer were obtained.

When the hologram is reconstructed, not only images of the phase object and the grating are recovered in all channels, but the whole sequence of self-reproductions of this grating. Therefore, in order to obtain a clear interference pattern, the fixing screen must be located in one of the planes of self-reproduction, the plane number being limited only by diffraction effects, which are especially pronounced for high spatial harmonics. At a great distance from the plane of the

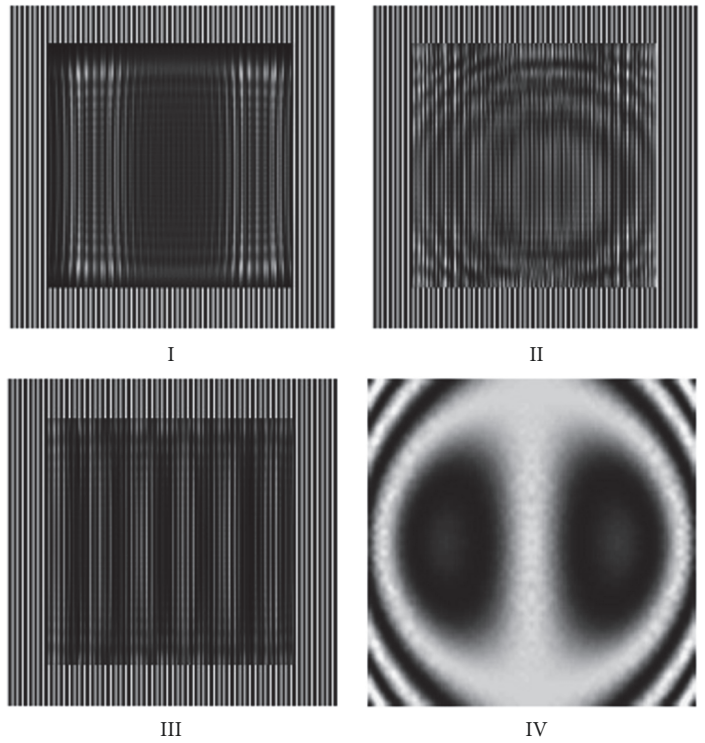

FIGURE 5: The object is lens with spherical aberration. The distance from the hologram to the interferogram plane is z = 8 z_T ($z_T = 2d^2/\lambda$, d is the grating period, λ is the wavelength). I, II, III, and IV output channels.

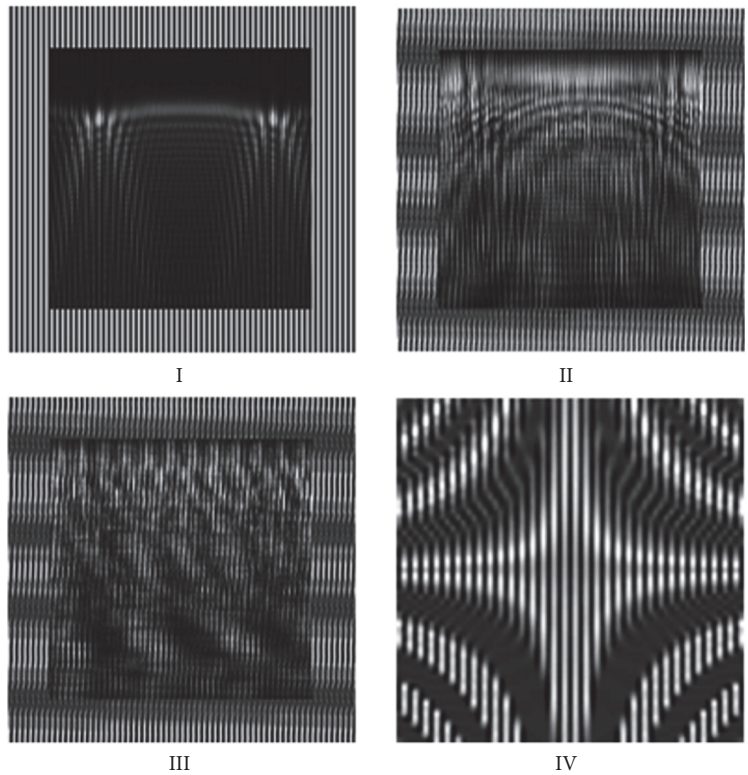

FIGURE 6: The object is the lens with coma. The distance from the hologram to the interferogram plane is z = 8 z_T. I, II, III, and IV output channels.

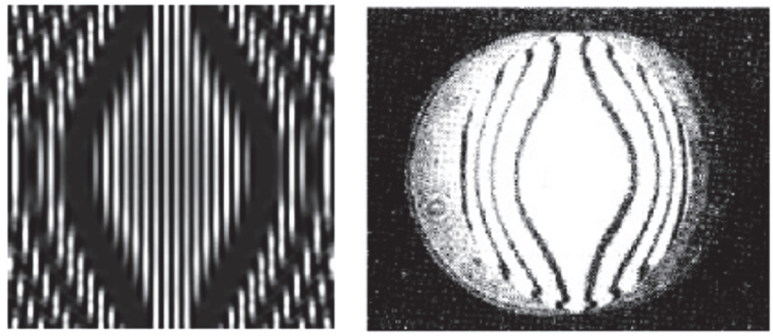

(a) (b)

Figure 7: Interferograms of lens having spherical aberration. The focal plane of the lens. (a) Computer simulation. (b) Optical analogy.

hologram, distortions of self-reproduction occur due to the fact that most of the high diffraction orders do not participate in the formation of the image.

The distance between the plane of location of the hologram and the plane of the screen was set in the values of the multiple Talbot constant $z_T = 2d^2/\lambda$, where d is the grating period, and λ is the wavelength.

In order to be able to compare interference patterns in the interferometer channels in the presence of a phase object and in its absence, each channel is represented as a sum of two pictures: the inner square is an interference pattern in the presence of a phase object; the area between the boundaries of the inner and outer squares is an interference pattern in the absence of a phase object, but under the same other conditions.

In Figures 5 and 6, as an illustration of the operation of a computer model of a multichannel holographic interferometer with a wide range of sensitivity, holograms obtained in the output channels of the interferometer are presented. Interferograms were obtained for a lens with the presence of aberrations. Figure 5 shows the interferograms of a lens in the presence of spherical aberration. When the hologram was restored, the grating in the restoring object wave rotated around an axis perpendicular to the grating plane. The angle between the lines of the original grating and the rotated one was $\beta = 0{,}06$ radian. The spherical aberration coefficient is A = 30 [30]. As can be seen from Figure 5, the presence of a phase object such as a lens forms a distorted image of the grating in channel I, at which the grating lines symmetrically shift from the central axis of the interference pattern and, at the same time, the grating period increases. This pattern of grating distortions is similar to the pattern of distortion of the grating lines in the Ronchi method [30]. The presence of spherical aberration leads to a curvature of the grating lines in the first channel. From these distortions, as in the Ronchi method, one can only qualitatively judge the presence of spherical aberration and, to some extent, its magnitude.

Channel IV gives a picture of moiré lines that are curved due to the presence of spherical aberration in a lens. The frequency of the moiré pattern and, therefore, the sensitivity of the channel can be adjusted by changing the angle between the lines of the original grating recorded on the hologram and the lines of the grating in the restoring wave. This channel, in fact, works like a classical Talbot interferometer.

Channels II and III form high-frequency interference pattern characteristic of holographic interferometers. These are channels of high sensitivity, allowing fixing the slightest oscillations of inhomogeneity of the phase medium under study.

Figure 6 shows interferograms of a lens with coma-type aberration. The aberration coefficient is B = 2 [30]. With the exception of coma, the characteristics of the lens and the conditions for obtaining interferograms are similar to the case of a lens with spherical aberration.

To substantiate the performance of a computer model of a multichannel interferometer, the results of computer simulation were compared with the results of optical experiments. Figures 7 and 8 compare the results obtained for a thin lens in the presence of spherical aberration and Figure 9 compares the results in the presence of a coma. The results of optical experiments are taken from the book of D. Malacara [30]. Figures 7(a) and 7(b) show the interferograms, obtained, respectively, on a computer model and in an optical experiment, for the spherical aberration coefficient A = 30. Interferograms are fixed in the focal plane of the lens.

In Figures 8(a) and 8(b), a comparison is also made for a lens with a spherical aberration coefficient A = 30, but the interferograms are fixed in planes located behind the focus of the lens.

Figures 9(a) and 9(b) show the interferograms for a lens with a coma. The aberration coefficient is B = 2; the interferograms are fixed in the focal plane.

Characteristics of this channel coincide with the characteristics of the conventional Talbot interferometer. The figures show a good coincidence of computer results and their optical analogies. But on Figures 7(a), 8(a), and 9(a) we see moiré distortion (distortion of two gratings as in the usual Talbot interferometer), and on Figures 7(b), 8(b), and 9(b) distortions of a separate grating are represented. So the computer results have grating lines which we do not see on optical figures.

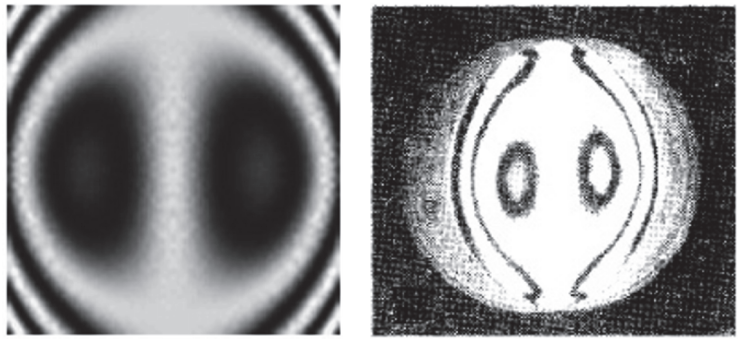

(a) (b)

Figure 8: Interferograms of lens with spherical aberration. The plane after focal plane of the lens. (a) Computer simulation. (b) Optical analogy.

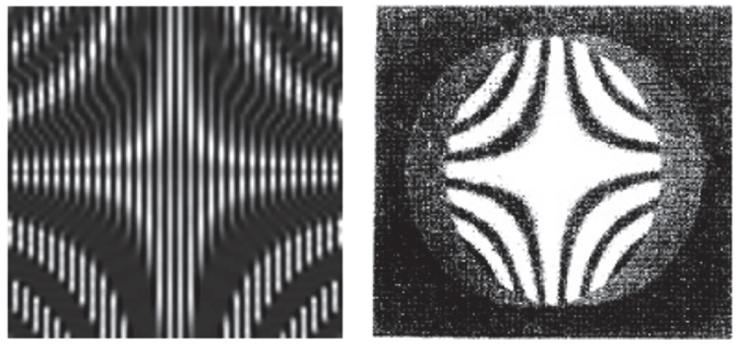

(a) (b)

Figure 9: Interferograms of a lens with coma. Focal plane of the lens. (a) Computer simulation. (b) Optical analogy.

4. Conclusions

The multichannel wide-range holographic interferometer developed on the base of holographic Talbot effect has wide range of sensibility and this range can be varied by means of spatial filtration. It is shown that this interferometer has four output channels, each of which has its own sensitivity value. In the first channel, the image of the linear grating, distorted by the phase object, is restored. This is a low-sensitivity channel, and it can be used to qualitatively evaluate the distribution of inhomogeneity in the object under study using the Ronchi method. The second and third channels are highly sensitive holographic channels, which make it possible to determine even insignificant changes in the values of the inhomogeneity of the phase medium. The fourth channel is similar in its characteristics to the conventional Talbot interferometer. In this channel, the distribution of the inhomogeneity is estimated mainly from the moiré pattern; i.e., this channel is less sensitive than the highly sensitive channels numbers II and III.

The results of computer simulation of a multichannel wide-range holographic interferometer have shown good possibilities for studying phase media. This is especially noticeable when considering relatively complex phase media for which the gradients of the variation in the inhomogeneity of the medium are not constant. The working capacity of the computer model of this interferometer is confirmed by a good coincidence of interference patterns obtained in channel IV, which has the characteristics of a conventional Talbot interferometer, with the patterns obtained by the same method for the Talbot interferometer, but optically.

Data Availability

All data used to support the results of this study are included in the article.

Conflicts of Interest

The authors declare that there are no conflicts of interest regarding the publication of this paper.

References

[1] P. Latimer, "Talbot plane patterns: Grating images or interference effects?" *Applied Optics*, vol. 32, no. 7, pp. 1078–1083, 1993.

[2] P. Latimer, "Use of the Talbot effect to couple the phases of lasers," *Applied Physics Letters*, vol. 62, no. 3, pp. 217-218, 1993.

[3] L. Liu, "Talbot and Lau effects on incident beams of arbitrary wavefront, and their use," *Applied Optics*, vol. 28, no. 21, pp. 4668–4677, 1989.

[4] R. Jozwicki, "The Talbot effect as a sequence of quadratic phase corrections of the object Fourier transform," *Optica Acta*, vol. 30, no. 1, pp. 73–84, 1983.

[5] J. Ebbeni, "Nouveaux aspects du phenomene de moire. I," *Nouvelle Revue d'Optique*, vol. 1, no. 5, pp. 333–342, 1970.

[6] Y. Nakano and K. Murata, "Measurements of phase objects using the talbot effect and moiré techniques," *Applied Optics*, vol. 23, no. 14, pp. 2296–2299, 1984.

[7] J. Wen, Y. Zhang, and M. Xiao, "The talbot effect: Recent advances in classical optics, nonlinear optics, and quantum optics," *Advances in Optics and Photonics*, vol. 5, no. 1, pp. 83–130, 2013.

[8] C. Zhang, W. Zhang, F. Li, J. Wang, and S. Teng, "Quasi-Talbot effect of a grating in the deep Fresnel diffraction region," *Journal of the Optical Society of America*, vol. 24, no. 6, pp. 1656–1665, 2007.

[9] J. Wen, S. Du, H. Chen, and M. Xiao, "Electromagnetically induced Talbot effect," *Applied Physics Letters*, vol. 98, no. 8, p. 081108, 2011.

[10] Z. Benkö, "New considerations on Talbot's bands," *American Journal of Physics*, vol. 68, pp. 513–519, 2000.

[11] D. E. Silva, "Talbot Interferometer for Radial and Lateral Derivatives," *Applied Optics*, vol. 11, no. 11, pp. 2613–2624, 1972.

[12] A. W. Lohmann and D. E. Silva, "An interferometer based on the Talbot effect," *Optics Communications*, vol. 2, no. 9, pp. 413–415, 1971.

[13] A. W. Lohmann and D. E. Silva, "A Talbot interferometer with circular gratings," *Optics Communications*, vol. 4, no. 5, pp. 326–328, 1972.

[14] K. Patorski, "Talbot interferometry with increased shear: part 3," *Applied Optics*, vol. 27, no. 18, pp. 3875–3878, 1988.

[15] L. Liu, "Interferometry based on the partially coherent effect lying between the talbot and lau effects," *Journal of Modern Optics*, vol. 35, no. 10, pp. 1605–1618, 1988.

[16] S. Yokozeki, "Electronic talbot interferometer," *Optics and Lasers in Engineering*, vol. 2, no. 1, pp. 13–19, 1981.

[17] M. J. Marques, A. Bradu, and A. Podoleanu, "Two-grating Talbot bands spectral-domain interferometer," *Optics Expresss*, vol. 40, no. 17, pp. 4014–4017, 2015.

[18] S. Pissadakis, "An elliptical Talbot interferometer for fiber Bragg grating fabrication," *Review of Scientific Instruments*, vol. 76, Article ID 066101, 2005.

[19] J. Kiyohara, C. Makifuchi, K. Kido et al., "Development of the Talbot-Lau interferometry system available for clinical use," in *Proceedings of the AIP Conference*, vol. 1466, pp. 97–102, 2012.

[20] H. Konitz, "Zur Frage der selbastalbildung (Talbot – effekt) Periodischer Objecte unter holographischen Bedingungen," *Optik - International Journal for Light and Electron Optics*, vol. 66, no. 3, pp. 197–204, 1984.

[21] H. Konitz, S. Boseck, and R. Lasch, "Holographischen Experimente zum Talbot – Effekt von Streifengittern," *Optik - International Journal for Light and Electron Optics*, vol. 69, no. 3, pp. 91–93, 1985.

[22] A. Maripov and Y. Ismanov, "The Talbot effect (a self-imaging phenomenon) in holography," *Journal of Applied Physics*, vol. 74, no. 12, pp. 7039–7043, 1993.

[23] S. Agarwal, V. Kumar, and C. Shakher, "Temperature measurement of wick stabilized micro diffusion flame under the influence of magnetic field using digital holographic interferometry," *Optics and Lasers in Engineering*, vol. 102, pp. 161–169, 2018.

[24] C. M. Vest, *Holographic Interferometry*, John Wiley and Sons, New York, NY, USA, 1979.

[25] T. Konishi, A. Ito, Y. Kudo et al., "Simultaneous measurement of temperature and chemical species concentrations with a holographic interferometer and infrared absorption," *Applied Optics*, vol. 45, no. 22, pp. 5725–5732, 2006.

[26] V. Kumar and C. Shakher, "Measurement of temperature and temperature profile of candle flame using holo-shear lens and Fourier transform fringe analysis technique," *Optical Engineering*, vol. 54, no. 8, article 084105, 2015.

[27] A. Maripov, Y. Ismanov, and K. Omyrzakov, "Four-channel wide-range holographic interferometer," *Proceedings of SPIE*, vol. 5144, pp. 606–610, 2003.

[28] A. Maripov and Y. Ismanov, "Interferometer based on the Talbot effect in holography," *Journal of Optics*, vol. 26, no. 1, pp. 25–28, 1995.

[29] Y. K. Ismanov and A. Maripov, "Holographic Talbot interferometer," *Proceedings of SPIE*, vol. 4149, pp. 213–220, 2000.

[30] D. Malacara, *Optical Shop Testing*, John Wiley and Sons, New York, NY, USA, 1982.